Extraction of the nuclear-spin diffusion constant from measurements of macroscopic heat transfer in small particles*

J. V. Gates, II and W. H. Potter

University of California, Physics Department, Davis, California 95616

(Received 11 August 1975)

Experiments are reported which measure the *macroscopic* transfer of energy from the surface of small particles to the interior via nuclear-spin diffusion at He temperatures. Adsorbed paramagnetic O_2 is responsible for the exchange of energy between the nuclear spins on the surface and the liquid-He bath. A theory of the decay of the cw-NMR signal is presented that allows a direct determination of the nuclear-spin diffusion constant. The proton-spin diffusion constant was determined by this method in yttrium ethyl sulfate and found to be $(4.3 \pm 0.3) \times 10^{-12}$ cm^2/sec.

I. INTRODUCTION

We have developed and experimentally tested in a variety of materials a theory of nuclear spin-bath relaxation in finely powdered insulators. If the concentration of magnetic moments of electronic origin within the material is sufficiently low, the nuclear-spin relaxation at temperatures of a few degrees or less is dominated by *macroscopic* diffusion of the magnetization to the surfaces of the particles. The nuclear spins at the surface are relaxed by adsorbed paramagnetic O_2. If a nuclear magnetization or polarization, characterized by a spin temperature T_I, is created, and T_I is not equal to the bath temperature, the observed decays of this polarization in samples of different particle size by cw-NMR yield the nuclear-spin diffusion constant in that material.

The concept of spin diffusion was first postulated in 1949 by Bloembergen[1] to explain how nuclear spins are brought into thermal equilibrium with the lattice phonons in insulators. The nuclear spins situated near an electronic magnetic impurity are relaxed to the lattice temperature by the fluctuating magnetic field of the impurity spin. The bulk of the nuclear spins, which are located more distantly from the impurity spins, are brought into equilibrium by the diffusion of Zeeman energy within the nuclear-spin system.

The general subject of nuclear spin-lattice relaxation in insulators is complicated and is still not completely understood. For example, it was only in the last few years that the very important role played by the electronic moment dipole-dipole reservoir in nuclear relaxation came to be understood and appreciated.[2]

Previous studies of the spin diffusion process itself involved trying to extract information about diffusion during the first several milliseconds of the decay in a nuclear spin-lattice relaxation experiment.[3-5] In these studies it was necessary to know the detailed distribution of the paramagnetic

ions. An exception is a recent study of diffusion in the field gradients of a type-II superconductor.[6] In this study too, however, the spin diffusion constant is extracted from the initial-time behavior during the first several milliseconds of the decay.

It was generally considered impossible to observe spin diffusion over macroscopic distances or measure the spin diffusion constant directly because of the smallness of the diffusion constant. However, for particles of the order of a few tens of microns in diameter or smaller, the macroscopic transport of Zeeman energy by spin diffusion to or from the surface can be and is observed[7] to be the dominant nuclear-spin relaxation mechanism.

In this paper we present a theoretical model that explains the observed decays of the proton polarization in samples of finely powdered crystals of $Y(C_2H_5SO_4)_3 \cdot 9H_2O$ (YES), $YCl_3 \cdot 6H_2O$ (YCl$_3$), and $La_2Mg_3(NO_3)_{12} \cdot 24H_2O$ (LMN). Direct evidence of the presence of O_2 on the surface and of its role in the surface relaxation is presented. We show that it is possible to obtain the spin diffusion constant from these results and we discuss the applicability of the method to the measurement of D in various materials. We find the value of D in YES to be $(4.3 \pm 0.3) \times 10^{-12}$ cm^2/sec.

II. EXPERIMENTAL

A. Measurement techniques and apparatus

All of the polarization decays were obtained by continuously monitoring the NMR absorption signal with a high-sensitivity cw bridge spectrometer employing a hybrid-T. Either the integral of the absorption signal, obtained electronically,[8] or the first Fourier component[9] of the absorption signal was recorded. Both methods gave identical decays. An advantage of the method using an electronic integrator is that small drifts in the magnetic field over periods of several hours have absolutely no effect on the recorded signal. With

the first-Fourier-component method, such drifts can change the observed signal amplitude, although much less than when one observes the absorption derivative.[9] The rf magnetic field was kept at a level such that the measured exponential decay due to rf saturation typically had a time constant of 20 h to several days. The temperature of the samples was 1.1 K and the magnitude of the applied magnetic field was between 5.5 and 6.0 kOe. The field was modulated at 17 Hz with a width typically three times the linewidth.

The samples were contained in cylindrical cells 9.5 mm in diameter and 25.4 mm long. The $\frac{1}{2}$-g sample occupied a region 7.9 mm in diameter and 20 mm long. Seven cells could be stacked end-to-end and attached to a plastic rod that passed through a vacuum seal in the top flange of the Dewar. The stationary NMR coil, 11.2 mm in diameter, was made to sample the various cells by raising or lowering the rod from outside the Dewar. Thus seven different samples, all of which had exactly the same history, could be observed in one experimental run. All of the materials in the vicinity of the rf coil, as well as the sample cells, were Kel-F, a fluorinated plastic which contains no hydrogen. The background proton signal, including any signal from adjacent cells, was typically 1% or less of the thermal equilibrium (TE) signal.

By doping the YES and YCl₃ with small amounts of Yb, usually 0.04 at.%, the proton polarization could be enhanced and become much greater than the TE value by the spin-refrigerator method.[10-13] The polarization was then monitored as it decayed to its TE value. Alternatively, the NMR signal was saturated and the buildup back to TE was monitored. The former method gave much larger signal-to-noise ratios, typically about 100–500, while the latter gave ratios of about 20–100. The effects of long-term drifts were also decreased by approximately a factor of 5 when enhanced signals were used. The rotating magnetic field required for the spin-refrigerator method was obtained by oscillating a 6-kOe air-core solenoid at 60 Hz. The solenoid was in the 15-cm gap of an electromagnet. The resultant of the static 6-kOe field from the electromagnet and the 6-kOe oscillating field rotates through an angle of 90° with an effective rotational speed that depends on the angle. This is not an optimum system for producing high proton polarization by the spin-refrigerator method, but it is a rather simple way of obtaining modest proton polarization enhancements. In this study the polarization buildup was always terminated at enhancements of less than 10.

B. Sample preparation

Single crystals[14] of the various salts were ground with a mortar and pestle and then sifted to obtain particles in definite size ranges. For particle sizes greater than 37 μm, standard sieves were used. Sieves made from electroformed nickel mesh[15] were used in the range 6–37 μm. Adsorbed water on the ground particles, as well as water pockets within the crystal that are exposed when the crystal was ground, can prevent successful sifting in the smaller size ranges. A rather simple solution to this problem is to do the grinding and sifting in a glove box which is continuously flushed with dry air. In addition, for the smallest sizes a small bell jar connected to a vacuum pump was used periodically to dry further the material as it was being sifted. All sifting was by hand.

More detailed particle-size ranges were determined later by actually measuring the diameters of a small fraction of the particles from the various sample cells used in the experiments. An optical microscope was used to make enough photomicrographs of a slide on which the sample was spread to get a representative sampling. Table I lists the measured size ranges for the particular samples. Since some of the samples are hygroscopic to some extent, the extremely low humidity in the vicinity of the laboratory area was very advantageous. No special handling techniques were necessary once the samples had been sifted, and samples kept in closed containers in a refrigerator were still dry many months later.

One set of samples of YES was ground in a nearly O₂-free atmosphere in order to examine the effect of the adsorbed O₂. Dry N₂ gas was continually flushed through the plastic glove bag, and the sample cells were loaded and sealed inside the bag. The seal around the sample cells was not broken until the cells had been lowered into the dry He atmosphere of the Dewar. This set of cells was subsequently removed from the Dewar, exposed to a mixture of N₂ and O₂, and reinserted in the Dewar.

III. THEORETICAL MODEL

A. Microscopic considerations

The diamagnetic ionic crystals used in these studies contain a nuclear-spin system and a small number of paramagnetic ions which form the electron-spin system. The abundant hydrogen nuclei in the waters of hydration and in the ethyl groups in YES constitute the nuclear-spin system. There are a few other nuclear moments present, but these can be neglected because their magnetic moment is much smaller than that of hydrogen and their number is very small compared to hydrogen.

We assume there is only one species of magnetic ion present. This is the case for the crystals doped with Yb or Dy. All magnetic moments are sufficiently far from one another so that they interact only through the magnetic dipole moment

TABLE I. Characteristics of YES samples.

Sample	Nominal	Measured radius distribution,[a] a^x					Doped	Run No.	Chemical batch No.
		Particle size—radius of spheres (μ m)							
A	19–22	13.5: 10%	19: 38%	24: 36%	31: 16%		yes	39	13–8
B	19–22	(Used size distribution of Sample A in Eq. 7)					yes	35	11–7
C	12–19	7.5: 10%	10: 14%	12.5: 38%	15: 38%		yes	38	13–8
D	12–19	6.5: 8%	9.5: 24%	12.5: 36%	15.5: 19%	19: 13%	no	37	13–7
E	8–12	2.5: 4%	5: 24%	7: 33%	9: 28%	10.5: 11%	no	37	13–7
F	8–12	5: 20%	7: 42%	9: 16%	10.5: 22%		yes	38	13–8
G	5–8	2: 9%	3: 22%	5: 35%	6.75: 34%		yes	39	13–8
H	5–8	{ G, H, and I different sample cells, but				}	yes	39	13–8
I	5–8	{ sifted together				}	yes	38	13–8
J	5–8	2: 16%	3.5: 33%	5: 37%	6.5: 13%		no	37	13–7
K	3–5	1.5: 11%	2.5: 33%	3.5: 33%	4.5: 23%		no	37	13–7
L	3–5	2: 27%	3: 36%	4: 20%	5: 17%		yes	38	13–8
M	106–125						yes	38	13–8
N	106–125						yes	39	13–8
P	75–85						yes	35	11–7
Q	106–125						no	37	13–7
R	75–85	(same sample cell as P)					yes	34/35	11–7
S	19–22	(same sample cell as B)					yes	34/35	11–7
T	0–19						yes	34/35	11–7
U	106–125						yes	38	13–8
V	37–45						yes	39	13–8
W	19–22						yes	23	5–1

[a]The percentages which follow the radius sizes are percentages of the sample volume comprised of particles of that radius.

and not by exchange or the "Coulomb" interaction.

The magnetic behavior of the crystal can be described by a spin Hamiltonian

$$\mathcal{H}_{spin} = \mathcal{H}_S + \mathcal{H}_I + \mathcal{H}_{SS} + \mathcal{H}_{II} + \mathcal{H}_{SI} ,$$

where $\mathcal{H}_S$ and $\mathcal{H}_I$ are the spin Hamiltonians of the electron-spin and nuclear systems respectively, and $\mathcal{H}_{SS}$, $\mathcal{H}_{II}$, and $\mathcal{H}_{SI}$ are the dipolar interactions between the electron spins, the nuclear spins, and the electron and nuclear spins, respectively.

In an applied magnetic field much larger than the local fields, the Zeeman interaction dominates any other term in $\mathcal{H}_{spin}$ and we speak of the electron and nuclear Zeeman systems (EZS and NZS). The three interaction terms in the spin Hamiltonian constitute the dipolar interaction system (DIS). These three thermodynamic systems can be assigned separate spin temperatures T_S, T_I, and T_D, respectively.[16]

In the macroscopic description of the decay of nuclear polarization in finely powdered crystals, we assume that the total effect of $\mathcal{H}_S$, $\mathcal{H}_{SS}$, and $\mathcal{H}_{SI}$ plus the interaction of the electron spins with the lattice is to cause the NZS to relax to the lattice temperature T_L at a rate independent of T_D.

This will be true if the heat capacity of the DIS is sufficiently small compared to that of the NZS. Under these circumstances, nuclear-spin diffusion, caused by the flip-flop transitions induced by terms in $\mathcal{H}_{II}$, causes any spatial inhomogenity in T_I to be

smoothed out over a time characteristic of the size of the particle and the magnitude of D. This process is described with a classical diffusion equation with D determined by $\mathcal{H}_{II}$.

If, however, the heat capacity of the DIS is not sufficiently small, then several additional complications arise. The NZS can relax to the DIS rather than directly to the tightly coupled EZS and lattice phonons. In this case the NZS and the DIS come to a common temperature and relax together to the lattice temperature. When T_I and T_D remain uniform on a macroscopic scale, but are made different from T_L by rapidly changing the applied field or by the application of microwave or rf fields, we have the various relaxation phenomena reviewed in Ref. 2. If, however, a *macroscopic* inhomogenity is created in T_I, as is the case in the experiments described in this paper, then spin diffusion in the DIS can occur. Since the NZS can be tightly coupled to the DIS, nuclear Zeeman energy can be transported over macroscopic distances by the much faster spin diffusion in the DIS. This can be significant, even though the heat capacity of the DIS is still much smaller than the heat capacity of the NZS, because the diffusion coefficient in the DIS is typically some 10^4–10^5 times larger than in the NZS. The diffusion coefficient is in general proportional to the square of the magnetic moment and to the inverse of the separation of the moments.

The experimentally accessible parameter that determines which regime is operative is the concentration of the paramagnetic ions. Experimental evidence for systems such as YCl_3 and LMN doped with rare-earth ions indicates that if the atomic concentration of the paramagnetic ion is much greater than about 0.01 at.%, the role of the DIS becomes important.[2,17] However, in the particular case of YES doped with Yb, the efficacy of the DIS in spatially redistributing nuclear Zeeman energy is reduced owing to the smallness of $g_\perp$, the g factor of the Yb ion in the direction perpendicular to the crystal axis. The terms in $\mathcal{H}_{SI}$ that connect the NZS and DIS together are proportional to $g_\perp$ and the terms in $\mathcal{H}_{SS}$ that cause diffusion of spin energy in both the EZS and the DIS are proportional to $g_\perp^2$. Since $g_\perp$ is smaller for Yb in YES ($g_\perp \approx 0.003-0.01$) than in any other known system, we should expect the effect of the DIS to remain negligible until the Yb concentration is considerably greater than the concentration at which the effect is important in all other systems for which $g_\perp$ is not essentially zero. This is the justification for neglecting spin diffusion in the DIS in the description of the nuclear polarization decays in YES doped with 0.04 at.% Yb. However, the effect of the DIS does have to be taken into account for a complete description of the decays in the LMN and YCl_3 samples.

B. Macroscopic description

We consider first the time development of the nuclear-spin polarization of an individual particle. There will be a normal spin-lattice relaxation rate, probably angularly dependent, characterized by the time constant $T_{1b}(\theta)$, where θ is the angle between the applied magnetic field and the crystal symmetry axis. This relaxation term is due either to unwanted paramagnetic impurities or to small concentrations of rare-earth ions intentionally introduced into the crystal. We are not concerned with the microscopic details of this process. On a macroscopic scale we require only that this process be independent of particle size. In fact, as we shall see, we do not even need to know $T_{1b}(\theta)$ to extract the diffusion constant.

The nuclear spins very near the surface are relaxed to the bath temperature by the fluctuating magnetic field of adsorbed paramagnetic oxygen molecules. If a polarization different from the TE value is created in the bulk spins, they will relax to the TE value by the action of both the normal spin-lattice relaxation process and by macroscopic spin diffusion to the surface.

As discussed in Sec. III A, we assume that nuclear-spin energy is *not* transported over macroscopic distances by the DIS, but only by spin diffusion within the NZS.

If the process that causes the non-TE polarization has a time constant that is very short compared to both $T_{1b}(\theta)$ and the time characteristic of the diffusion to the surface, it is possible to create a relatively spatially uniform polarization in the interior of the particle. Thus the initial condition will be a step function; $P_{surf}(t) = P_0$ and $P(\vec{r}, t=0) = EP_0$, where P_0 is the TE polarization and E is the enhancement factor, which can be either smaller or larger than unity. In our case, values of E larger than unity are achieved with the spin refrigerator and values of E much less than unity by rf saturation. The differential equation describing the polarization after the initial condition is established is

$$\frac{dP(\vec{r}, t)}{dt} = \frac{P_0 - P(\vec{r}, t)}{T_{1b}(\theta)} + D\nabla^2 P(\vec{r}, t) , \qquad (1)$$

and we assume D to be adequately described as a scalar.

The validity of the step function for the initial condition is verified by solving the equation[18]

$$\frac{dP(\vec{r}, t)}{dt} = \frac{\beta P_0 - P(\vec{r}, t)}{T_i(\theta)} + \frac{P_0 - P(\vec{r}, t)}{T_{1b}(\theta)}$$

$$+ D\nabla^2 P(\vec{r}, t), \qquad (2)$$

where βP_0 is the polarization that would be reached due either to the spin refrigerator or the rf saturation in the absence of spin-bath with a build up time $T_i(\theta)$, with initial condition $P(\vec{r}, t=0) = P_0$ and the boundary condition $P_{surf}(t) = P_0$ for the time t_i equal to the length of time either the spin refrigerator or the high-power rf was turned on. For the actual values of t_i, T_i, and β used in the experiments, the solution of Eq. (2) is approximated very well by a step function.

It is necessary to assume a particular particle geometry before proceeding further with the solution of Eq. (1). We have carried the analysis through to the extraction of D for both spherical and cubical particles. The value of D obtained from the same experimental data using cubical particles with the cube edge equal to the diameter of the sphere is about 15% higher than for spherical particles. Since the actual particles of YES resemble spheres more than cubes, we use spherical particles for the analysis. The uncertainty in the values of D caused by this effect is discussed further in Sec. V.

For a spherical geometry, the boundary condition becomes $P(R, t) = P_0$, where R is the radius of the particle, and the solution of Eq. (1) is

$$P(\vec{r}, t) = P_0 + \left[2[1 - E(\theta)] P_0 \exp\left(\frac{-t}{T_{1b}(\theta)}\right) \right]$$

$$\times \sum_{n=1}^{\infty} (-1)^n R \frac{\sin(n\pi r/R)}{n\pi r} \exp\left(\frac{-n^2\pi^2 Dt}{R^2}\right). \quad (3)$$

Since the observed signal is the average polarization of the particles, it is necessary to average Eq. (3) over r and θ. The average polarization of a single particle oriented at an angle θ with respect to the applied field is

$$P_c(R, \theta, t) = P_0 + \left[6P_0[E(\theta) - 1]\exp\left(\frac{-t}{T_{1b}(\theta)}\right)\right]$$

$$\times \sum_{n=1}^{\infty} \frac{1}{n^2\pi^2}\exp\left(\frac{-n^2\pi^2 Dt}{R^2}\right). \qquad (4)$$

The sample polarization is obtained by averaging Eq. (4) over θ and using an appropriately volume-weighted distribution of R's. Note that all of the θ dependence in Eq. (4) appears in the factor in the large square brackets which is independent of R. The sample polarization thus becomes

$$P_s(\alpha, R, t) = P_0 + \Theta(t)$$

$$\times \sum_i \left[\alpha_i \sum_n \frac{1}{n^2\pi^2}\exp\left(\frac{-n^2\pi^2 Dt}{R_i^2}\right)\right], \qquad (5)$$

where $\Theta(t)$ is the angular average of the quantity in large square brackets in Eq. (4) and α_i is the percentage of the total volume comprised of particles with radius R_i. The α_i's and R_i's correspond to the actual particle-size range of the sample in the particular experiment.

Because there was always a few percent of the sample volume with R of the order of a few microns, it was convenient to normalize all observed decays to a time t_n such that the polarization of these small particles had essentially reached P_0. The validity of this is discussed further in Sec. V. The observed decay normalized at time t_n is thus

$$\mathscr{P}(\alpha, R, t_n, t) = \frac{P_s(\alpha, R, t) - P_0}{P_s(\alpha, R, t_n) - P_0} = f(t_n, t)\frac{\sum_i \alpha_i \sum_n n^{-2}\exp(-n^2\pi^2 Dt/R_i^2)}{\sum_j \alpha_j \sum_p p^{-2}\exp(-p^2\pi^2 Dt_n/R_j^2)}, \qquad (6)$$

where $f(t_n, t) = \Theta(t)/\Theta(t_n)$.

The function $f(t_n, t)$ is independent of particle size. It is thus possible to eliminate $f(t_n, t)$ by taking the ratio of the decays of two samples X and Y. The resulting function is

$$F(\alpha^X, R^X, \alpha^Y, R^Y, t_n, t) = \frac{\mathscr{P}(\alpha^X, R^X, t_n, t)}{\mathscr{P}(\alpha^Y, R^Y, t_n, t)} = \frac{\sum_i\{\alpha_i^X \sum_n n^{-2}\exp[-n^2\pi^2 Dt/(R_i^X)^2]\}\sum_l\{\alpha_l^Y \sum_q q^{-2}\exp[-q^2\pi^2 Dt_n/(R_l^Y)^2]\}}{\sum_k\{\alpha_k^Y \sum_m m^{-2}\exp[-m^2\pi^2 Dt/(R_k^Y)^2]\}\sum_j\{\alpha_j^X \sum_p p^{-2}\exp[-p^2\pi^2 Dt_n/(R_j^X)^2]\}}. \qquad (7)$$

The function $F(\alpha^X, R^X, \alpha^Y, R^Y, t_n, t)$ is obtained experimentally simply by taking the ratio of two normalized sample decays. The value of D is used as an adjustable parameter to make Eq. (7) fit the experimentally obtained F. Since the particle-size ranges are measured, there are no adjustable parameters or unknowns in Eq. (7) other than D. In particular, there is no dependence on the normal spin-lattice relaxation, concentration of paramagnetic impurities, or any of the subtle microscopic effects normally associated with nuclear spin-lattice relaxation. All of these effects are present to the same extent in both samples and consequently do not appear in the ratio.

In the practical application of Eq. (7) it is desirable that F change with time as rapidly as possible. This is accomplished by making R^Y large enough so that the decay of this sample is due primarily to spin-lattice relaxation and by making R^X small enough so that macroscopic diffusion is predominant.

It is not necessary to reproduce single sample decays in order to obtain D. However, the decay of a single sample is decribed by Eq. (6). The function $f(t_n, t)$ can be obtained if the possibly angle-dependent enhancements and spin-lattice relaxation rates are known. If the enhancement has no angular dependence, as in the case of strong rf saturation, $f(t_n, t)$ is simply the ratio of the averaged decays,

$$f(t_n, t) = \frac{\langle \exp[-t/T_{1b}(\theta)]\rangle_{av}}{\langle \exp[-t_n/T_{1b}(\theta)]\rangle_{av}}. \qquad (8)$$

The angular dependence of the relaxation rates can be obtained from data on single crystals. It is necessary to scale the rates of samples made from different chemical batches, using one adjustable parameter to take into account any differences in the paramagnetic impurity concentration between the single crystal and the powdered samples made from different batches.

We now examine the effect on the decays if there is not enough O_2 on the surface to keep the surface polarization at P_0. The amount of Zeeman spin energy that must be transferred to or from the lattice by the O_2 at the surface is proportional to the total number of nuclear spins and thus to the volume of the particle. Hence the amount of energy that must be transferred by a single O_2 molecule is proportional to the volume-to-surface ratio, which varies as R. This energy is transferred in a time that also depends on the size of the particle. From the argument of the exponential in Eq. (3), for example, we see that the time needed to transfer a

given amount of energy to the surface is proportional to R^2. Then the rate at which a single O_2 molecule must transfer the nuclear Zeeman energy is proportional to $R/R^2 = 1/R$. This means that the O_2 must be more efficient in transferring Zeeman energy on a small particle than on a large particle in order to keep the surface polarization at P_0. In terms of the amount of O_2 on the surface, more is required for smaller particles. Consequently, as the amount of adsorbed O_2 is decreased, we would expect to see a reduced polarization decay rate in the smallest particles first.

IV. EXPERIMENTAL RESULTS

Extensive data were taken on samples of YES to explore the validity of the theoretical model. YES was chosen for two reasons. It was available with very low concentrations of paramagnetic impurities,[14] e.g., at 1.1 K and in a field of 6 kOe, the spin-lattice relaxation time of undoped YES was measured to be greater than 3 days. By doping YES with small concentrations of Yb, enhanced polarizations could be obtained while the spin-lattice relaxation times were kept on the order of 5 hours. Some data were also taken on samples of YCl_3 and LMN, primarily to verify that this effect was not

FIG. 1. Ratios of polarization decays in YES. Sample characteristics and sizes are given in Table I. Solid lines are calculated using Eq. (7) with the value of D adjusted to give the best fit for each pair. These values of D are listed in Table II.

peculiar to YES. More qualitative data were also obtained on the fluorine spins in CaF_2 and Teflon. (Future experiments are planned to measure accurately the spin diffusion constant in CaF_2 by this method.)

A. YES

Table I summarizes the details of the various samples. The particle-size distributions of samples A and $C-L$ as measured with a microscope are listed by volume percentages. These are calculated with the assumption that the particles are spheres. The exact sizes of the larger particles are not critical in the analysis. Typically, 300 individual particles were measured to obtain these distributions. The nominal sizes listed are one-half the screen openings in the sieves that bracketed the particular sample, and correspond to the radii of the particles, assumed to be spherical. The doped samples contain 0.04-at. % Yb substituted for the Y atoms.

1. Diffusion constant in YES

In order to obtain the diffusion constant, the ratios of pairs of decays were plotted as shown in Fig. 1. The data points were obtained by taking the ratio of the normalized value of the polarization of the two indicated samples. All of the decays used in Fig. 1 were normalized at $t_n = 1600$ sec. The solid lines were obtained from Eq. (7) by using the measured α's and R's and varying D to obtain the best fit. The average R of the nominal size range was used for the larger particles since diffusion to the surface is small compared to the normal spin-lattice relaxation. Both members of the pair used in a ratio in Fig. 1 were from the same run and were ground from the same batch of single crystals. The greater amount of scatter in the data of the ratios of the sample pairs D/Q, E/Q, J/Q, and K/Q is due to the fact that they were obtained from rf saturation recovery rather than from decay from an enhanced polarization to the TE value. The values of D obtained from the data of Fig. 1 are listed in Table II.

2. Effect of O_2 on surface

In Fig. 2, we show the decays of three sample cells which were run on consecutive days. The samples were ground and sifted in a nearly O_2-free environment and run the first day. These data are the circles in Fig. 2. The next day, the samples were withdrawn, exposed to a 50%-O_2-50%-N_2 atmosphere and reinserted in the still-cold Dewar. The decays after exposure to O_2 are represented by squares and triangles. The degree of reproducibility of the data is seen in the two decays of sample R after exposure to O_2. The squares of sample R were taken before S and T and the triangles of

TABLE II. Sample pairs X and Y for determination of D.

Sample pair	Nominal sizes (μ m)	$D(10^{-12}$ cm^2/sec)	Doped
A/N	19–22/106–125	3.8	yes
B/P	19–22/75–85	4.25	yes
C/M	12–19/106–125	3.8	yes
D/Q	12–19/106–125	4.7	no
E/Q	8–12/106–125	4.1	no
F/M	8–12/106–125	4.4	yes
G/N	5–8/106–125	4.2	yes
H/N	5–8/106–125	4.2	yes
I/N	5–8/106–125	4.2	yes
J/Q	5–8/106–125	4.1	no
K/Q	3–5/106–125	3.9	no
L/M	3–5/106–125	4.5	yes

sample R were taken afterwards, about 7 hours having elapsed. These decays are normalized to unity at the start of the decay. Apparently the amount of adsorbed O_2 on the surface of the particles was reduced enough to make a difference in the decay of sample T, but not enough to show a change in the larger-particle samples.

3. Long-time polarization decays

Several polarization decays that were observed over many hours are shown in Fig. 3. The solid curves are $P(\alpha, R, t_n, t)$ from Eq. (6). These decays are interesting because they show clearly the varying importance of the several factors that determine the decay, namely diffusion to the surface, spin-lattice relaxation, and rf saturation. Sample Q is undoped YES; consequently it decays much more slowly than the others. The decays of samples V and B illustrate how the shape of the decay depends on the relative strength of the various processes. The decay of sample V is much closer to being a single exponential than is B. The particle
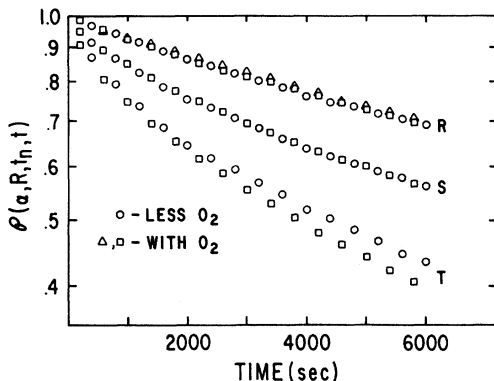
FIG. 2. Decays of three sample sizes in YES o, before, and □ and △ after exposure to O_2. The decreased amount of adsorbed O_2 affects only the smallest particles, sample T.
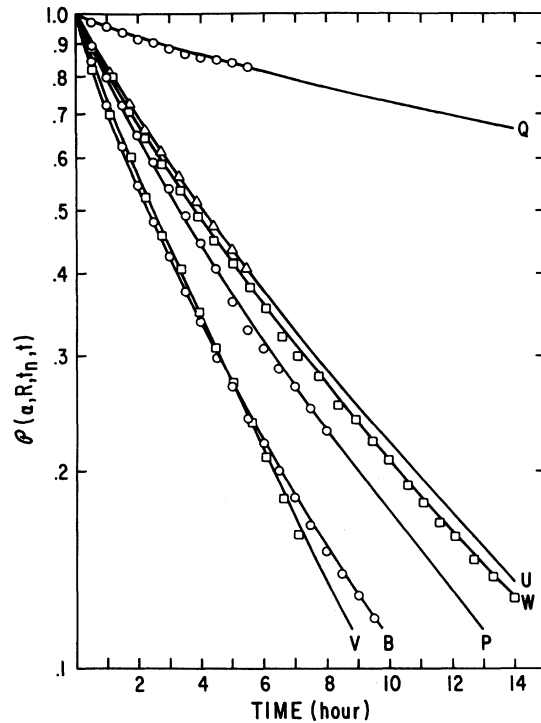
FIG. 3. Proton polarization decays in YES observed for long times. Solid lines are calculated using Eq. (6) and the parameters listed in Tables III and IV.

size of B is actually smaller than that of V. However, a greater rf saturation of V, which has but a single rate rather than the sum of rates due to diffusion, causes it to decay faster and with nearly a single exponential rate. The difference in the decays of B and P is due only to particle size. For particles identical in other respects to B and P but large enough so that diffusion to the surface is negligible, the decay would be just below that shown for sample W.

In order to use Eq. (6) to fit these decays it is necessary to know the function $f(t_n, t)$, which is basically the angular average of the spin-lattice relaxation rates. The spin-lattice relaxation rate can be written as $T_{1b}^{-1}(\theta) = Ck(\theta)$, where C is a concentration-dependent scale factor and $k(\theta)$ incorporates the intrinsic angular dependence. For all samples from a given chemical batch, C is a constant. In Table III are listed the values of C as well as the normalization times for the decays shown in Fig. 3. The average of $\Theta(t)$ was performed by summing $k(\theta)$ over 20 discrete intervals which were chosen such that there were an equal number of particles in each interval. The $k(\theta)$ for each interval were experimentally determined from the angle-dependent spin-lattice relaxation rate of a single crystal of Yb-doped YES. The dimensions of the single crystal are the order of

TABLE III. Characteristics of samples shown in Fig. 3.

Sample	Chemical batch No.	Run No.	C	t_n (sec)
B	11–7	35	0.00047	1800
P	11–7	35	0.00047	1800
Q	13–7	37	0.00005	400
U	13–8	38	0.00040	1600
V	13–8	39	0.00040	1600
W	5–1	23	0.00035	2000

several mm, so macroscopic diffusion plays no observable role in the relaxation. Table IV lists the $k(\theta)$ corresponding to the angular intervals.

When the polarization was enhanced by the spin refrigerator, only particles with $\theta \gtrsim 45°$ were affected, since the total magnetic field oscillated through a limited angle. This effect is rather well accounted for by treating the enhancement E as a step function of magnitude E for $45° \le \theta \le 90°$ and as unity for $0 \le \theta < 45°$.

The following procedure was used for fitting Eq. (6) to the data: If the rf saturation rate was known experimentally to be negligible, then the $k(\theta)$'s as given in Table IV contain the angular dependence. For the largest-particle-size sample, diffusion to the surface is small relative to spin-lattice relaxation, so the decay is not sensitive to the exact value of D. Thus, using a reasonable value of D, the constant C was varied to give a best fit to the decay of the largest particle size. This value of C was then used for all other samples from the same chemical batch. In the case of sample V, in which it was known that there was rf saturation, a constant rate was added to the $k(\theta)$. This rate was determined by comparing other decays of sample U from runs 38 and 39. The rf saturation time constant corresponding to this rate was 15.5 hours and is consistent with the known power level and characteristics of the sample probe.

B. LMN and YCl$_3$

In Table V we list some of the materials other than YES for which data were collected and the value of D obtained using Eq. (7). These values of D do *not* correspond to the nuclear-spin diffusion val-

ue in these materials. The reason is that they all had relatively fast spin-lattice relaxation rates, indicating that the heat capacity of the DIS is large enough to transport nuclear Zeeman energy by spin diffusion in the DIS. The LMN was nominally undoped, but was made with water that had a rather high concentration of transition-metal impurities. In all cases, however, the general pattern of faster decays with smaller particles was always observed.

V. ANALYSIS AND CONCLUSIONS

We now examine the assumptions made in the theoretical model and discuss the applicability of this model to the data on YES. The underlying assumption that the nuclear polarization at the surface is held at the TE value by adsorbed O_2 is strongly supported by the data shown in Fig. 2. It was shown in Sec. III that as the amount of O_2 on the surface of the particles was reduced, the assumption fails first for the smallest particles; the effect is proportional to $1/R$. This is exactly what is seen in Fig. 2. The decay of sample T, the smallest of the three sizes, is definitely slower with less O_2 on the surface. This sample contained all particles that passed a 37-μm-opening sieve, so that a significant fraction of the particles had diameters of less than, say, 10 μm. It is this fraction that is responsible for the difference between the decays before and after exposure to O_2. On the other hand, the larger-particle-size samples are unaffected because even with the reduced level of O_2 there is enough O_2 to keep the surface polarization at the TE value.

It is difficult to make any quantitative estimate of the actual amount of O_2 required to keep the surface polarization at the TE value. However, it is possible to estimate the probable coverage of adsorbed O_2 from air at NTP. From data on the adsorption of O_2 at NTP on silica gel[19] and NaCl,[20] we estimate a coverage of about 1/100 of a complete monolayer. This corresponds to an average O_2 spacing of about 37 Å. In contrast, a 1-at. % doping of paramagnetic ions in YES corresponds to a paramagnetic ion spacing of about 50 Å. Thus it is not unreasonable that the amount of O_2 ad-

TABLE IV. Rates used to evaluate the angular average of $\Theta(t)$.

θ (deg)	k (sec^{-1})	θ	k	θ	k
0–18.2	0.048	49.5–53.1	0.345	72.5–75.5	0.225
18.2–25.8	0.155	53.1–56.6	0.318	75.5–78.5	0.192
25.8–31.8	0.233	56.5–60.0	0.309	78.5–81.4	0.157
31.8–36.9	0.305	60.0–63.3	0.309	81.4–84.3	0.109
36.9–41.4	0.347	63.3–66.4	0.309	84.3–87.1	0.092
41.4–45.6	0.371	66.4–69.5	0.272	87.1–90	0.923
45.6–49.5	0.382	69.5–72.5	0.245		

TABLE V. Characteristics of other samples.

Material	Nominal size radius (μ m)	Effective D ($\times 10^{-12}$)	Relaxation time of large particles (sec)
YCl_3: 0.04-at.%-Yb	19–22/75–88	11	7200
YCl_3: 0.004-at.%-Dy	19–22/75–88	72	1200
LMN	8–12, 12–19, 19–22/106–125	30	600

sorbed from the atmosphere at NTP can in general keep the surface polarization at P_0.

Several approximations and procedures used in fitting Eq. (7) to the data of Fig. 1 need further explanation. By normalizing all decays to unity 1600 sec after the saturating rf or spin refrigerator was turned off, the effects of a small volume percentage of particles about 1 μm in diameter are almost eliminated. This has no effect on the value of D obtained from Eq. (7) provided that the distribution of actual particle radii of the sample is adequately represented by the discrete α's and R's. Figure 4 shows the data for the sample pair B/P normalized to 0, 1200, 3600, and 6000 sec. The solid line is Eq. (7) with the same value of D used for each decay. For this sample, D is certainly independent of t_n in the range $1200 \le t_n \le 6000$. However, for all of the samples, particularly the smaller sizes, the value of D was not independent of t_n for t_n less than 800 sec, because the α's corresponding to the smaller R's could not be determined with enough precision. This is seen in Fig. 4 for the fit with $t_n = 0$. The data drop below the theoretical curve over the first part of the decay. It is for this reason that we used $t_n = 1600$ sec. For this normalization time, four discrete α's for the smaller sample and one for the larger is sufficient.

If the particle shapes are similar in the different samples so that the use of spherical geometry is equally valid, then any difference in the value of D determined from different sample sizes is due mainly to error in the determination of the discrete α's and R's. Uncertainties in the TE values of particular decays give a much smaller uncertainty in D than does the uncertainty in α and R. We consider this to be random error, and average the values of D obtained from all sample pairs.

To check on the assumption that the DIS is not transporting nuclear Zeeman energy over macroscopic distances in YES we can compare the average D obtained from the doped and undoped samples. The averages are $(4.17 \pm 0.25) \times 10^{-12}$ and $(4.20 \pm 0.35) \times 10^{-12}$ cm²/sec, respectively. At this level of doping, the Yb spins apparently act individually to increase the proton spin-lattice relaxation rate, but do not act collectively in any significant way. Thus we believe the average value

$(4.18 \pm 0.27) \times 10^{-12}$ cm²/sec represents the best value of the proton diffusion rate based on the assumed spherical geometry.

On the other hand, the particles could be treated as cubes with the cube edge equal to twice the radius of the sphere, and the data of Fig. 1 analyzed accordingly. The values one then obtains for D are slightly higher, ranging from 4.5×10^{-12} cm²/sec for the larger particles to about 5.3×10^{-12} cm²/sec for the smaller ones. Since the shape of the ground particles appeared under a microscope to be much closer to spheres than cubes, the value of D quoted above will be a lower limit, although very close to the true value. The fact that there is no trend in the fitted values of D with particle size using the spherical model, as there is when one uses cubes, further supports the spherical model. We thus believe the proton diffusion coefficient in YES is $D = (4.3 \pm 0.3) \times 10^{-12}$ cm²/sec. It should be noted that the value $D = 5 \times 10^{-12}$ cm²/sec quoted in our earlier preliminary report[7] was obtained using only one R for each size range. This tends to weight the larger R's too heavily. When the true distribution of R's was used to evaluate that data, the value of D dropped into the range 4.25×10^{-12} cm²/sec.

If the protons in YES are assumed to be distributed uniformly on a cubic lattice, one can calculate the value of D using the formula of Lowe and Gade[21] to be $D = 4.1 \times 10^{-12}$ cm²/sec. A calculation of D based on the exact position of the 66 protons in the YES unit cell is underway.[22]

The over-all correctness of the theoretical model is further demonstrated by the fits of Eq. (6) to
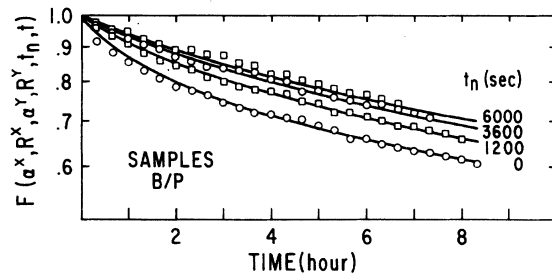
FIG. 4. Ratio of decays B and P normalized at various times. All solid lines are calculated using Eq. (7) with $D = 4.25 \times 10^{-12}$ cm²/sec.

the data of Fig. 3. These long-term decays are completely described by Eq. (6) when angle-dependent normal spin-lattice relaxation is taken into account. We emphasize that no adjustable parameters are used in these fits other than the paramagnetic impurity-concentration-dependent factor, which is determined from *one* decay for each chemical batch. For example, the sample decays labeled B and P in Fig. 3 are from samples prepared from the same chemical batch, 11-7. Only the measured values of α and R are different in Eq. (6).

The decays of YCl_3 doped with Yb and Dy and the nominally undoped LMN can be fitted with Eq. (6) using a value of D obtained from Eq. (7). These decays are listed in Table V. However, this value of D is not representative of proton spin diffusion, but includes the effect of the much faster spin diffusion in the DIS. This is particularly evident in the YCl_3 decays. With Dy doping the effective D is about seven times larger than with Yb doping, and the spin-lattice relaxation rate is a about six times larger with Dy doping. Since the value of $g_\perp$ for Dy in YCl_3 is larger than for Yb, and both are larger than $g_\perp$ for Yb in YES, it is

reasonable that the effect of the DIS is largest in the Dy-doped samples, even though the concentration is down by a factor of 10. In the case of LMN there is apparently a significant amount of magnetic impurities present, as evidenced by the very short relaxation time of 600 sec. Thus the value of D quoted is certainly not representative of proton spin diffusion.

Similar behavior was also observed in the decays of the ^{19}F polarization in samples of Teflon particles and CaF_2. Studies are underway to use this technique to study spin diffusion in the DIS itself. However, it is clear that in order to measure the nuclear-spin diffusion coefficient in a material using the method described in this paper, it is necessary to have samples very free of magnetic impurities. This ensures that the DIS does not contribute to the diffusion process and that macroscopic spin diffusion is not obscured by spin-lattice relaxation.

ACKNOWLEDGMENT

*Work supported in part by the Research Corporation.

[1] N. Bloembergen, Physica (Utr.) 15, 386 (1949).

[2] W. Th. Wenckebach, T. J. B. Swanenburg, and N. J. Poulis, Phys. Rep. 14, 181 (1974).

[3] W. E. Blumberg, Phys. Rev. 119, 79 (1960).

[4] D. Tse and I. J. Lowe, Phys. Rev. 166, 292 (1968).

[5] G. W. Leppelmeier and J. Jeener, Phys. Rev. 175, 498 (1968).

[6] A. Z. Genack and A. G. Redfield, Phys. Rev. Lett. 31, 1204 (1973).

[7] J. V. Gates, II and W. H. Potter, Phys. Rev. Lett. 33, 878 (1974).

[8] W. H. Potter (unpublished).

[9] W. H. Potter, Rev. Sci. Instrum. 45, 1288 (1974).

[10] K. Langley and C. D. Jeffries, Phys. Rev. 152, 358 (1966).

[11] J. R. McColl and C. D. Jeffries, Phys. Rev. B 1, 2917 (1969).

[12] W. H. Potter and H. J. Stapleton, Phys. Rev. B 5, 1729 (1972).

[13] H. B. Brom and W. J. Huiskamp, Physica (Utr.) 60, 163 (1972).

[14] J. V. Gates, II and W. H. Potter (unpublished).

[15] The nickel mesh was purchased from Buckbee-Mears Co., St. Paul, Minn. 55101.

[16] A general discussion of the dipolar interaction system and justification for treating it as a separate thermodynamic system is given in Ref. 2.

[17] H. B. Brom and W. J. Huiskamp, Physica (Utr.) 63, 599 (1973).

[18] J. V. Gates, II (unpublished).

[19] D. M. Young and A. D. Crowell, *Physical Adsorption of Gases* (Butterworths, London, 1962), p. 376.

[20] J. W. McBain, *The Sorption of Gases and Vapors by Solids* (Routledge, London, 1932), p. 252.

[21] I. J. Lowe and S. Gade, Phys. Rev. 156, 817 (1967).

[22] J. V. Gates, II (unpublished).